Selection of Comprehensive Design Criteria

for Highway Bridges in the Vicinity of and Crossing

Active Faults

Maria I. Todorovska (Principal Investigator)

Mihailo D. Trifunac (Co-Principal Investigator)

School of Engineering/Department of Civil Engineering

University of Southern California

Los Angeles, California 90089-2531

METRANS
Transportation Center
USC / CSULB

DISCLAIMER

The contents of this report reflect the views of the authors, who are responsible for the facts and the accuracy of the information presented herein. This document is disseminated under the sponsorship of the Department of Transportation, University Transportation Centers Program, and California Department of Transportation in the interest of information exchange. The U.S. Government and California Department of Transportation assume no liability for the contents or use thereof. The contents do not necessarily reflect the official views or policies of the State of California or the Department of Transportation. This report does not constitute a standard, specification, or regulation.

ABSTRACT

The earthquake induced transient forces in bridge structures are due to the simultaneous action of *dynamic* (inertia) forces caused by ground shaking, and *quazi-static* forces caused by oscillatory differential motions of the supports due to the wave passage. The *dynamic* forces are those that are normally considered in seismic design. For bridges that cross faults, which are not uncommon in California, in addition to the transient forces, *static* forces may also be induced by permanent offset on the fault. The static forces have been considered separately, usually in deterministic analyses. In this work, the action of all three types of forces is considered, within the framework of probabilistic seismic hazard analysis. The output of the analysis consists of uniform hazard relative displacement spectra for columns for given probability of being exceeded during specified exposure period (the life or service time of the structure).

The methodology is presented and demonstrated for three sites in southern California, using a hypothetical but realistic model for the earthquake sources. The relative significance of each of the three effects is analyzed for each site. All three are located on a fault, one on a smaller fault (Class B), and two on a major fault along the plate boundary (Class A). The results show that the transient differential motions contribute to the hazard significantly for stiffer structures, with periods $T < 1$ s, while, for more flexible structures, the hazard for transient motions is governed by the dynamic response. The differential motions are more significant for longer distances between the supports and for softer ground. The fault displacement hazard dominates for very small probabilities of being exceeded ($p = 0.01$ for the three case studies). Its contribution to the hazard rapidly decreases with increasing probability of being exceeded, becoming eventually insignificant (for $p > 0.3$ for the three case studies).

The presented methodology is relevant for: (a) *deign and retrofit* of bridges near and crossing earthquake faults, (b) *seismic risk assessment* for the ground transportation system, i.e. the risk for physical damage, loss of function, and overall economic consequences on the regional economy, and (3) *emergency planning*.

TABLE OF CONTENTS

APPEDIX A

Todorovska M.I., Trifunac M.D., Lee V.W. (2007). Shaking hazard compatible methodology for probabilistic assessment of permanent ground displacement across earthquake faults, *Soil Dynamics & Earthquake Engrg*, **27**(6), 586–597.

APPEDIX B

Todorovska M.I., Trifunac M.D. (1996). Hazard mapping of normalized peak strain in soil during earthquakes: microzonation of a metropolitan area, *Soil Dynamics & Earthquake Engrg*, **15**(5), 321-329.

APPEDIX C

Trifunac M.D., Lee V.W. (1989). Empirical models for scaling pseudo relative velocity spectra of strong earthquake accelerations in terms of magnitude, distance, site intensity and recording site conditions, *Int. J. Soil Dynamics & Earthquake Engrg*, **8**(3), 126-144.

LIST OF FIGURES

Fig. 12   Same as Fig. 11 but for probability of being exceeded $p = 0.1$ in 50 years. The Fault Displacement level for the same probability is also shown.

Fig. 13   Same as Fig. 11 but for probability of being exceeded $p = 0.01$ in 50 years. The Fault Displacement level for the same probability is also shown.

Fig. 14   Site 3: Uniform Hazard Spectral Displacement $SD(T)$ for $\zeta = 5\%$ and for probabilities of being exceeded $p = 0.01$, 0.1, 0.5, 0.9 and 0.99 in 50 years. The Fault Displacement levels for probabilities of being exceeded $p = 0.01$, 0.1, 0.2 and 0.3 are also shown.

Fig. 15   Site 3: Spectral Displacement $SD(T)$, and Spectral Displacement for Columns for longitudinal and transverse motions, $SDC_L(T,\zeta,\tau)$ and $SDC_T(T,\zeta,\tau)$ for $\zeta = 5\%$ and for probability of being exceeded $p = 0.5$ in 50 years.

Fig. 16   Same as Fig. 15 but for probability of being exceeded $p = 0.1$ in 50 years. The Fault Displacement level for the same probability is also shown.

Fig. 17   Same as Fig. 15 but for probability of being exceeded $p = 0.01$ in 50 years. The Fault Displacement level for the same probability is also shown.

LIST OF TABLES

DISCLOSURE

Project was funded in entirety under this contract to California Department of Transportation.

ACKNOWLEDGEMENTS

1. INTRODUCTION

The seismic action on long structures on multiple supports, such as highway bridges, is a combination of (i) *dynamic forces* - due to inertia of the structure, and (ii) *quazi-static forces* - due to transient (oscillatory) differential motion of the supports, caused by the propagation of seismic waves. Bridges crossing a fault, which is not uncommon in California, are also exposed to the action of (iii) *static* forces due to permanent displacement across the fault from a seismic slip. Bridges should be designed considering the action of all forces. The following describes these three types of forces.

(i) The dynamic forces are proportional to the *relative* displacement of the structure (i.e. of the deck of the bridge) with respect to that of the ground, assumed to be synchronous at all supports, and the relative displacement is proportional to the *ground acceleration*. For such forces, structures are designed using a design spectrum, which is a form of a smoothed response spectrum.

(ii) The quazi-static forces are proportional to the relative displacements between the individual supports at a particular instant of time. The oscillatory differential motions, on level ground, are proportional to the ground strains, which are proportional to the *ground particle velocity*. The relative significance of these two types of forces for a particular structure depends on the natural period of the structure, distance between the supports, and type of ground. For example, in flexible structures (with long period *T*), which would experience larger relative displacement when subjected to synchronous motion of the supports, the quazi-static forces may be small compared to the dynamic forces. However, that is not the case for stiffer structures (with short period *T*) on separate supports (Trifunac and Todorovska, 1997). Such stiffer structures are e.g. highway overpasses, thousands of which exist in California. During the 1994

Northridge earthquake, six bridges collapsed, leading to a complete closure of the corresponding freeway lanes, and consequent traffic delays and financial losses. For four of the collapsed bridges, the failure mechanisms directly point to the absence of design criteria to consider such differential motions.

(iii) The static forces for bridges that cross an earthquake fault occur as follows. During an earthquake, the blocks of rock on the opposite sides of the fault slip relative to each other, resulting in permanent displacement of the ground on one side of the fault relative to the other side. For a larger earthquake, this displacement can be of the order of several meters. Examples of bridges crossing a fault include the Vincent Thomas Bridge (connecting Terminal Island and Port of Los Angeles to San Pedro), which crosses the Palos Verdes Fault, and the San Diego-Coronado Bay Bridge (connecting Coronado to San Diego), which crosses a number of strands of the Rose Canyon Fault Zone. Considering the rapid growth of the west coast ports and metropolitan areas in the U.S., and the increasing density of the ground transportation system to accommodate that growth, there will be more such structures in the futures. Such large differential displacements are likely to cause severe damage of bridges and possibly collapse, if not accounted for in design. Such damage was observed in Turkey from the 1999 Duzce earthquake ($M = 7.2$) and in Taiwan from the 1999 earthquake ($M = 7.6$). Severe damage of bridges during an earthquake would cause interruption of service on selected routs, and consequently monetary losses, e.g. loss of revenues on toll bridges, as well as economic losses to the broader community. Also, some of these bridges and tunnels may be of critical importance for emergency response, and must be designed so that they are operational after an earthquake. Therefore, it is important that design criteria for such structures include these loads.

We addressed the third (static) type of forces in our previous METRANS project, in which we developed a probabilistic hazard model for prediction of permanent ground displacement across a fault during the life of the structure, consistent with shaking hazard scaling models (Todorovska and Trifunac, 2006; Todorovska et al. 2007). In this work, we consider *all three* types of forces simultaneously, within the framework of probabilistic seismic hazard analysis, to be used in defining comprehensive design criteria for bridges near and crossing faults. The results are expressed in the form of a single uniform hazard spectrum, such that accounts for the three factors. Such a concept is novel in earthquake resistant design.

The major difference between the fault displacement hazard and that from ground shaking is that the former is due to a *single* fault (crossed by the bridge), while the latter is due also to many other faults that are sufficiently close to the bridge site. Consequently, the geographic location of the site relative to the major faults and the seismic activity on these faults are major factors affecting the relative significance of the three types of forces. The local site conditions also may enhance the relative contribution of the transient forces. Finally, the bridge characteristics, such as its natural period of vibration and its length affect the relative significance of the dynamic forces relative to the quazi-static and static forces. Conducting the analysis leading to the specification of the design motions within the framework of probabilistic seismic hazard analysis ensures that the degree to which the design accommodates each of these three types of forces is balanced.

This report is organized as follows. Chapter 2 presents the methodology, Chapter 3 presents demonstration of the methodology for three sites in southern California and analysis of the relative contribution of the tree types of motion. The assumed seismicity model is hypothetical but realistic. Finally, Chapter 4 presents the conclusions.

2. METHODOLOGY

2.1 Transient Motions – Spectral Displacement for Columns, $SDC(T,\zeta,\tau)$

The transient forces are due to the combined action of dynamic forces and differential motions assumed in this study to be caused only by transient ground strains. The action of the differential motions on a multiple-span bridge is illustrated in Fig. 1, for shorter waves propagating along the longitudinal axis of the bridge. Parts a) and b) correspond to out-of-plane and in-plane particle motions.
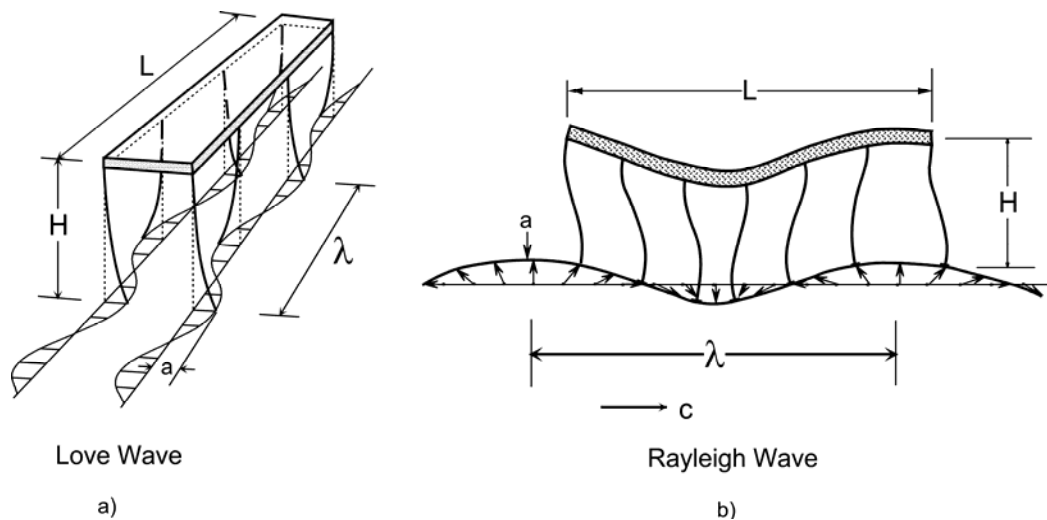
Fig. 1 A structure excited by the passage of (a) SH or Love waves, and (b) Rayleigh wave.

The in-plane motion can be decomposed into longitudinal, vertical, and rocking components, while the out-of-plane motion can be decomposed in transverse, rocking (about the longitudinal bridge axis), and torsion (along the vertical axis). Trifunac and Todorovska (1997) analyzed the effects of *horizontal* in-plane differential motion for buildings and bridges using a model similar to the one in Fig. 1b, and showed that the first-order effects can be accounted for by modification of the standard response spectrum. Later, Trifunac and Gičev (2006) extended this approach to

out of plane response (Fig. 1a). The new spectra are *relative displacement* type spectra, referred to as "spectral displacement for columns", $SDC_L(T, \zeta, \tau)$ and $SDC_T(T, T_T, \zeta, \zeta_T, \tau)$, where the subscript L and T indicate longitudinal and transverse motion, T and ζ are the natural period of vibration and damping ratio for the corresponding component of motion, T_T and ζ_T are the torsional period of vibration and corresponding damping ratio, and τ is time delay of the motion of the base of a particular column relative to the motion of a central point.

Trifunac and Todorovska (1997) and Trifunac and Gičev (2006) presented the following combination rules, which require specification only of peak values rather than time histories, and are, therefore, convenient for implementation in probabilistic seismic hazard analysis

$$SDC_L(T, \zeta, \tau) \approx \left\{ SD^2(T, \zeta) + \left(v_{\max}\tau\right)^2 \right\}^{1/2} \qquad \text{for in-plane motion} \qquad (1)$$

$$SDC_T(T, T_T, \zeta, \zeta_T, \tau) \approx \left\{ SD^2(T, \zeta) + 2\left(v_{\max}\tau\right)^2 \right\}^{1/2} \quad \text{for out-of-plane motion} \qquad (2)$$

where $SD(T, \zeta)$ is the standard relative displacement amplitude spectrum, and $v_{\max}$ is the peak ground velocity. The combination rule in Eqns (1) and (2) assumes that the occurrence of the peak spectral displacement and of the peak ground velocity is statistically independent. The time delay τ can be estimated from

$$\tau \equiv \frac{sx}{\beta_{av}} \qquad (3)$$

where β_{av} is the average shear-wave velocity in the top layer of soil, in general different from $V_{S,30}$ (Lee and Trifunac, 2010), s is an empirical scaling factor that is of order of unity (Trifunac and Todorovska, 1997), and x is the distance of the particular column from a central

point in the structure (or a bridge). Typical values of τ are less than 0.1. In Eqn. (2), it was assumed that $T \approx T_T$ and $\zeta \approx \zeta_T$.

The shape of $SDC_L(T, \zeta, \tau)$ is illustrated in Fig. 2 (redrawn from Trifunac and Todorovska, 1997) for recorded motion during the Northridge earthquake of January 17, 1994 (horizontal motion recorded at station USC#53). The backbone curve corresponds to $SD(T, \zeta)$. It can be seen that the differential motions are significant for stiffer structures (smaller T) and for larger values of delay time τ.

Once the SDC spectra have been evaluated, the maximum shear force V_{max} can be computed

$$V_{max} \approx k \, SDC \tag{4}$$

where k is the stiffness of the column.

For prediction from a possible future earthquake, $SD(T, \zeta)$ can be estimated using regression models for pseudo spectral velocity response spectrum amplitudes $PSV(T, \zeta)$, which are readily available

$$SD(T, \zeta) = \frac{T}{2\pi} PSV(T, \zeta) \tag{5}$$

or directly using a spectral displacement empirical scaling model (Lee, 2002; Trifunac, 1978; Trifunac and Lee, 1989; Lee and Trifunac, 1995). Similarly, v_{max} can be estimated by a ground motion prediction equation for peak velocity (Trifunac, 1976, Lee et al., 1995).
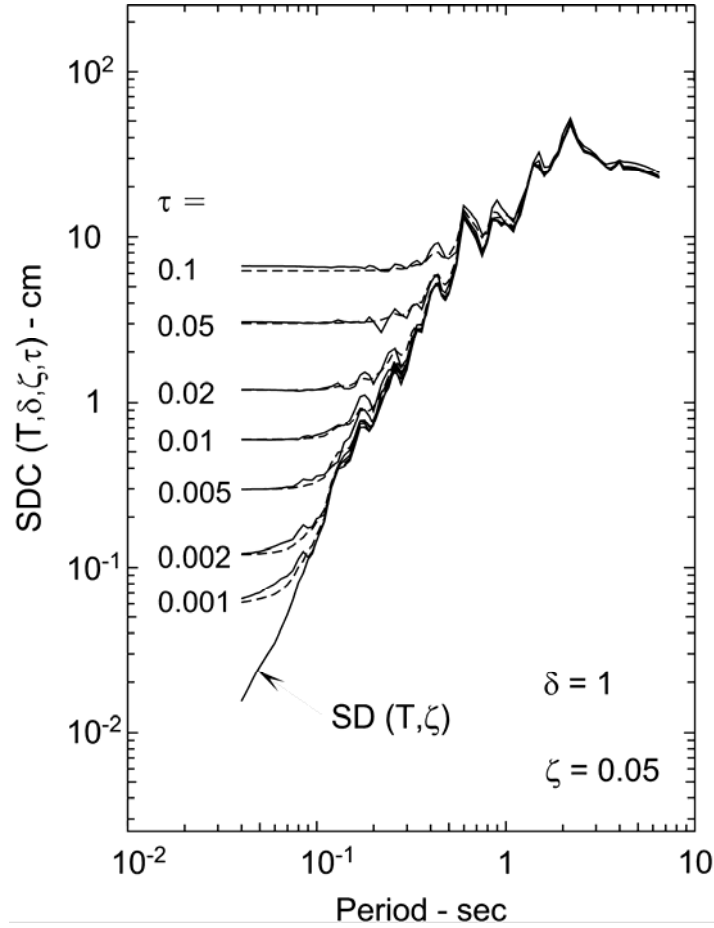
Fig. 2 Example of a Relative Displacement Spectrum for Columns, $SDC(T,\zeta,\tau)$, for longitudinal motion, computed for a scenario earthquake (redrawn from Trifunac and Todorovska, 1997).

2.2 Probabilistic Seismic Hazard Analysis Framework

Without loss of generality, we consider a Poissonian model of the earthquake occurrence. According to this model, the occurrences of the earthquakes on different source segments and with different magnitudes, even on the same segment, are statistically independent. For practical purposes, let us discretize the magnitudes of possible earthquakes on a fault, and let M_i be the magnitude corresponding to the i-th interval. Further, let $N_i(t)$ be the number of earthquakes

7

with magnitude M_i occurring during exposure t, and let $n_i(t) = E[N_i(t)]$, where $E[\cdot]$ indicates expected value. If $N_i(t)$ is a Poissonian random variable, then the return period of these earthquakes is an exponential random variable. Let Y be a random variable describing a particular effect of the earthquake at the site, and let $q(y)$ be the conditional probability that Y exceeds level y when an earthquake with magnitude M_i occurs

$$q_i(y) = P\{Y > y \mid \text{event } M = M_i \text{ occurred}\} \tag{6}$$

In eqn (6), $P\{\cdot\}$ indicates probability of occurrence of the event in the brackets. The event $\{Y > y\}$ is a selective Poissonian process, with rate that is a prorated value of the earthquake occurrence rate because not every earthquake that occurs necessarily produces the event. Because of the statistical independence of the events with different magnitudes, the rate of occurrence of event $\{Y > y\}$ from any magnitude earthquake is

$$m(y,t) = E\{Y > y \mid t\}$$
$$= \sum_{i=1} q_i(y) n_i(t) \tag{7}$$

The return period of $\{Y > y\}$ is exponentially distributed, and the probability that $\{Y > y\}$ occurs during exposure t is

$$p(y,t) = P\{Y > y \mid t\}$$
$$= 1 - e^{-m(y,t)} \tag{8}$$

For design, of interest are levels y_p such that will not be exceeded with given probability p, or the levels associated with a given return period of event $\{Y > y\}$. The level y_p is found as the root of the equation

$$p(y_p, t) = P\{Y > y_p | t\} \qquad (9)$$

If random variable Y is a function of the period of vibration T, then $y_p(T)$ constitutes a *uniform hazard spectrum*.

2.3 Uniform Hazard Relative Displacement Spectra for Columns, $SDC(T,\zeta,\tau)$

As seen from Section 2.2, the computation of uniform hazard $SDC(T,\zeta,\tau)$ spectra requires a probability distribution function. Such function can be obtained, in principle, by special regression analyses for $SDC(T,\zeta,\tau)$, like those for the peak amplitudes and spectral amplitudes of ground motion, which are not available at this time. Instead, regression models are available for $\log_{10} PSV(T)$ and $\log_{10} v_{\max}$, including a probability distribution functions for each one, which are not Gaussian. The combination rules in Eqns (1) and (2) can be applied, strictly speaking, to the expected values of $\log_{10} PSV(T)$ and $\log_{10} v_{\max}$. Because $\log_{10} PSV(T)$ and $\log_{10} v_{\max}$ have the same distribution, we assume that these rules can be extended to values of $\log_{10} PSV(T)$ and $\log_{10} v_{\max}$ with equal probability of being exceeded, and estimate approximately the hazard at the site.

Let $\log_{10} SDC(T,\zeta,\tau; p,t)$ be the value of $\log_{10} SDC(T,\zeta,\tau)$ that will be exceeded with probability p during the exposure t. We obtain $\log_{10} SDC(T,\zeta,\tau; p,t)$ for in-plane and out of plane motion from

$$\log_{10} SDC_L(T,\zeta,\tau; p,t) \approx \frac{1}{2}\log_{10}\left\{10^{2\log_{10} SD(T,\zeta;p,t)} + 10^{2[\log_{10} v_{\max}(p,t)+\log_{10}\tau]}\right\} \tag{10}$$

$$\log_{10} SDC_T(T,T_T,\zeta,\zeta_T,\tau; p,t) \approx \frac{1}{2}\log_{10}\left\{10^{2\log_{10} SD(T,\zeta;p,t)} + 10^{2\left[\log_{10} v_{\max}(p,t)+\log_{10}\left(\sqrt{2}\,\tau\right)\right]}\right\} \tag{11}$$

where $\log_{10} SD(T,\zeta; p,t)$ and $\log_{10} v_{\max}(p,t)$ are the values of $\log_{10} SD(T,\zeta)$ and $\log_{10} v_{\max}$ that will be exceeded with probability p during the exposure t.

2.4 Uniform Hazard Displacement Spectra for Structures Crossing Faults

For structures crossing a fault, the contribution from the static displacement caused by faulting must be added. It is important to note that, even if the site is on the fault, only some of the ruptures extend to the site, and affects the site in terms of static displacement. This can be seen in Fig. 3, which shows the model for probabilistic fault displacement hazard used in our previous METRANS project (Todorovska et al., 2007). Part a) shows a fault with length L and width W, dipping at angle δ, and extending from the ground surface to depth $H = W \sin \delta$. Part b) shows the fault surface, the site, and three possible ruptures, one of which affects the site, another one that occurs at depth and does not break the ground surface, and a third one that breaks the ground surface but does not extend horizontally to the site. The possible ruptures have lengths $L_R(M)$ and widths $W_R(M)$, which both depend on the earthquake magnitude.
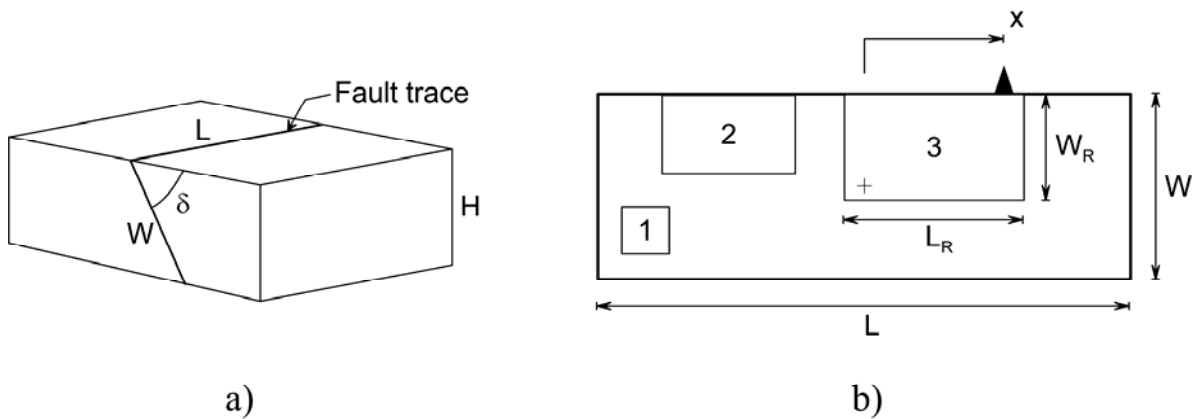

Fig. 3   Model for assessment of fault displacement hazard.

Let D_{Site} be a random variable representing the permanent displacement at the site caused by faulting. Then the conditional probability

11

$$q_i(d) = P\{D_{\text{site}} > d \mid \text{event } M = M_i \text{ occurred}\}$$

$$= P\{D > d \mid \text{event } M = M_i \text{ occurred }\} \tag{12}$$

$$P\left\{\begin{matrix}\text{rupture breaks}\\ \text{ground surface}\end{matrix}\right\} P\left\{\begin{matrix}\text{rupture extends}\\ \text{horizontally to the site}\end{matrix}\right\}$$

where D is a random variable representing the slip on the fault. The product of the latter two probabilities on the right hand side of Eqn (12) gives the probability that a rupture on that fault would affect the bridge site. These two probabilities were computed based on rupture length $L_R(M)$ and rupture width $W_R(M)$ predicted by empirical scaling models, specific for California, derived using data presented in Wells and Coppersmith (1994). The models for $L_R(M)$ and $W_R(M)$, as well as a model for $\log_{10} D$ and its probability distribution function are presented in Todorovska et al. (2007). Then, the probability of exceeding level d during the exposure

$$p(d,t) = P\{D_{\text{site}} > d \mid t\} \tag{13}$$

can be computed, as shown previously in Section 2.2.

The degrees to which the fault displacement affects the bridge in-plane and out-of-plane responses depends on the orientation of the bridge relative to the fault trace. If the bridge is almost parallel to the fault, the in-plane response will be most affected but not the out-of-plane one. Assuming that the occurrence of static displacement is statistically independent from the occurrence of the peak spectral displacement, and peak ground velocity, the combination rule for the total relative displacement at the site is

$$\log_{10} SDC_L^{Tot}(T,\zeta,\tau;p,t) \approx \frac{1}{2}\log_{10}\left\{\begin{matrix}10^{2\log_{10} SD(T,\zeta;p,t)} + 10^{2[\log_{10} v_{\max}(p,t)+\log_{10}\tau]}\\ +10^{2[\log_{10} D_{Site}(p,t)+\log_{10}\alpha]}\end{matrix}\right\} \tag{14}$$

$$\log_{10} SDC_T^{Tot}(T,T_T,\zeta,\zeta_T,\tau;p,t) \approx \frac{1}{2}\log_{10}\left\{ \begin{array}{l} 10^{2\log_{10} SD(T,\zeta;p,t)} + 10^{2\left[\log_{10} v_{max}(p,t)+\log_{10}\left(\sqrt{2}\,\tau\right)\right]} \\ + 10^{2\left[\log_{10} D_{Site}(p,t)+\log_{10}\beta\right]} \end{array} \right\} \quad (15)$$

where $D_{Site}(p,t)$ is the level of D_{Site} that will be exceeded with probability p during exposure t, and α and β are factors that have values between 0 and 1, depending on the orientation of the bridge relative to the fault. If the bridge is almost parallel to the fault, $\alpha = 1$ and $\beta = 0$, and if it is perpendicular to the fault, $\alpha = 0$ and $\beta = 1$.

2.5 Scaling Models

The empirical scaling models for $PSV(T)$, v_{max} and D are lengthy and are not presented in the main body of this report. Instead, appendices are included which reproduce publications presenting the full detail of these models. Appendix A presents our paper on fault displacement hazard (Todorovska et al., 2007), Appendix B presents our paper on probabilistic mapping of peak ground strain on level ground, via peak ground velocity (Todorovska and Trifunac, 1996), and Appendix C presents a paper summarizing models of $PSV(T)$ (Trifunac and Lee, 1989).

3. RESULTS AND ANALYSIS

The methodology is illustrated for three hypothetical sites located in a seismic region with overall seismicity comparable with the seismicity in southern California. Site 1 is chosen to lie on the trace of a Type B fault (away from the plate boundary) and Sites 2 and 3 lie are chosen to lie on the trace of a Type A fault (on the plate boundary, characterized by higher seismicity and capacity to generate larger earthquakes).   The results were produced by a new module of the NEQRISK software package, which computes peak transient relative displacements, $SDC_L(T,\zeta,\tau)$ and $SDC_T(T,\zeta,\tau)$, and, where appropriate, peak total relative displacements, $SDC_L^{Tot}(T,\zeta,\tau)$ and $SDC_T^{Tot}(T,\zeta,\tau)$, for a given seismicity model and site, and for chosen scaling models for response spectra, peak velocity and fault displacement from among the many models built in the package (Anderson and Trifunac, 1978; Lee and Trifunac, 1985; Trifunac, 1990; Todorovska and Trifunac, 1996; 1999; Todorovska et al., 2007). The exposure period is t = 50 years.

3.1 Seismic Sources Model Used

The model for the seismic sources is the same as the one used in our earlier work on mapping of liquefaction opportunity (Todorovska and Trifunac, 1999). Fig. 4 shows the location of the earthquake source zones, 32 of which are buried lines along the traces of the major faults, and two are diffused zones of point sources buried at depth over the areas enclosed by the dashed lines. Table 1 shows their names, seismic moment rates $\dot{M}_0$ and maximum magnitudes M_{max}. The moment rates are consistent with those for the alternate model (Poissonian) proposed by the working group on California earthquake probabilities (WGCEP, 1995). Two populations of earthquakes were assumed on each fault, referred to as "distributed" and "characteristic", both

14

occurring randomly in time as Poissonian sequences but on different magnitude ranges and with different rates. More details about the model can be found in Todorovska and Trifunac (1999). Fig. 5 shows the agreement of the overall seismicity rates for the region, accounted for by this model, with the Alternate Model of WGCEP (1995), and with rate observed since 1850 ($M \geq 6$, aftershocks removed). In this figure, $n(M)$ is the number of earthquakes per year with magnitude $\geq M$. The close agreement with the observed seismicity demonstrates that the model used in this study is realistic.
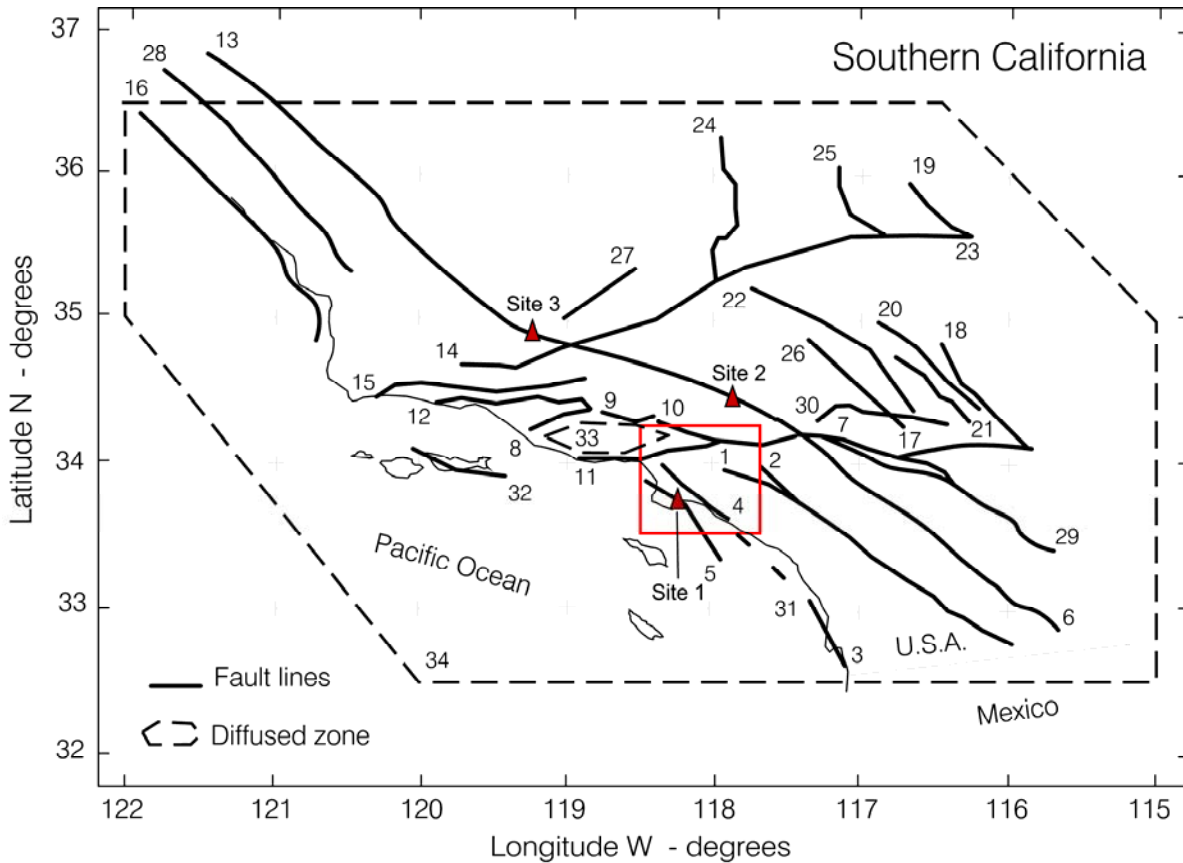

Fig. 4 Map of the faults of the Southern California Seismicity Model used for the examples in this report (Table 1). The locations of the three sites where the hazard is computed are also shown (redrawn from Todorovska and Trifunac, 1999).

Table 1 Southern California Seismicity Model – hypothetical but realistic seismic moment rates and maximum magnitudes for two populations of earthquakes, "distributed" and "characteristic" (redrawn from Todorovska and Trifunac, 1999).

Fault name (1)	$M_0^d \times 10^{22}$ (dyn-cm/year) (2)	$M_0^c \times 10^{22}$ (dyn-cm/year) (3)	M_{max} (4)
Elsinore-Whittier Fault	54	317	7.8
Chino Fault	5	15	7.4
Rose Canyon Fault	17	15	7.4
Newport-Inglewood Fault Zone	17	24	7.3
Palos Verde Fault	28	50	7.6
San Jacinto Fault Zone	75	811	7.9
San Andreas, Cajon Pass to Imperial Valley on North Branch	50	780	8.0
Oakridge Fault	44	0	7.6
Santa Susana Fault	22	2	7.5
Sierra Madre-Cucamonga Fault Zone	63	18	7.8
Malibu Coast-Santa Monica-Raymond Fault System	30	24	7.6
Arroyo Parida-San Cayetano Fault Zone	89	0	7.8
San Andreas Fault-Cajon Pass to San Luis Obispo	189	3,497	8.0
Big Pine Fault	13	0	7.4
Santa Ynez Fault	83	0	7.6
San Gregorio-Hosgri Fault Zone	61	25	7.7
Pinto Mountain Fault	18	1	7.3
Pisgan-Bullion Fault	32	0	7.7
South Death Valley Fault	43	0	7.7
Calico-West Calico Fault	32	0	7.7
Camp Rock-Emerson Fault Zone	32	0	7.7
Lockhart-Lenwood Fault	32	0	7.7
Garlock Fault	128	169	8.0
Sierra Nevada Fault	37	0	7.6
Panamint Valley Fault	44	0	7.7
Elendale Fault	32	0	7.8
White Wolf Fault	106	0	7.8
Rinconada Fault	39	0	7.4
San Andreas, Cajon Pass to Imperial Valley on South Branch	50	780	8.0
North Frontal Fault	31	0	7.0
Santa Cruz Fault	19	6	7.5
Newport-Inglewood Fault-Offshore	13	15	7.4
Simi-San Fernando Zone	21	57	7.3
Diffused Seismicity Zone	1,493	0	7.5

[a]For distributed and characteristic earthquakes M_0^d and M_0^c, respectively, and maximum magnitude M_{max}.
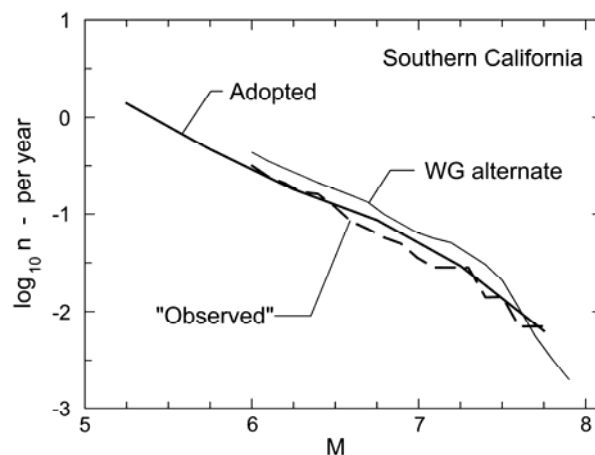

Fig. 5 Gutenberg-Richter relationship (cummulaive) for the Sothern California seismicity model adopted in this paper (see Fig. 4 and Table 1; redrawn from Todorovska and Trifunac, 1999), and comparison with the Alternate Model of WGCEP (1995), and with the rate observed since 1850 ($M \geq 6$, aftershocks removed).

3.2 Site Characteristics

The characteristics of the three sites (geographical coordinates and site conditions) are summarized in Table 2. The location of the sites, relative to the earthquake faults, is also shown in Fig. 4.   As it can be seen in Fig. 4, Site 1 is located on the Palos Verdes Flt, in San Perdo Bay, while Sites 2 and 3 are located on the segment of the San Andreas Flt between Cajon Pass and San Louis Obispo. Site 2 is located near the south end, while Site 3 is located near the center of the fault segment. Although Sites 2 and 3 lie on the same fault, both the hazard for the transient motions and fault displacement hazard are expected to be different, because of the different proximity to the other faults, which contribute to the former, and because of the differences in the distance from the possible ruptures on the fault, and the likelihood that a possible rupture will extend to the site (see Section 2.4).

The site geology is specified by two variables, one characterizing the deeper geology, and the other one characterizing the near surface soil. For Site 1, the deeper geology is described by the depth of sediments (depth to basement rock), which is assigned value H =2.4 km, while for Sites 2 and 3, it is described by the geologic site condition parameter, s, which is assigned value s =1, corresponding to "intermediate geology", i.e. geology that cannot be clearly described either as "sediments" or as "geologic rock".   The shallower geology is described by the local soil parameter s_L. At Site 1, s_L =2, which corresponds to "soft soil" and at Sites 2 and 3, s_L =1, which corresponds to "stiff soil".   This characterization of the local site conditions is compatible with the scaling models for response spectra and peak velocity used in this study (Trifunac, 1976; Trifunac and Lee; 1989).

17

Table 2 Geographic location and site conditions for the three sites

	Site 1	Site 2	Site 3
Coordinates	118.255˚W 33.74˚N	117.844˚W 34.438˚N	119.251˚W 34.871˚N
Geology	Depth of sediments H =2.4 km	s =1 ("intermediate geology")	s =1 ("intermediate geology")
Soil conditions	s_L =2 ("soft soil")	s_L =1 ("stiff soil")	s_L =1 ("stiff soil")

3.3 Scaling Models Used

For the examples shown, the following particular scaling models were used. The PSV spectra, needed to estimate the SD spectra (see eqn (5)), were predicted for Site 1 by the MAG-DEPTH-SOIL and for Sites 2 and 3 by the MAG-SITE-SOIL models of Trifunac and Lee (1989).   The peak particle velocity, $v_{\max}$, needed to estimate the transient peak differential motions, was computed for Site 1 by the MAG-DEPTH model (Todorovska and Trifunac, 1996), and, for Sites 2 and 3, by the MAG-SITE of Trifunac (1976).   Finally, the fault displacement was predicted by the same model for peak displacement at zero distance used previously in our study of fault displacement hazard (Todorovska et al., 2007). For all the models same magnitude-rupture length relationship was used, which is the one used in (Todorovska et al., 2007).

Further, for the fault displacement hazard, it was assumed that the ruptures occur on a vertical plane fitted so that it passes through the end points on the trace of the fault (Fig. 4). The fault length, L, and distances of the site from the center of the fault trace, x_c, used in the calculations for Site 1 on the Palos Verdes Flt were: L=73.7 km and x_c= 9.35 km. For Sites 2

and 3, which are on a segment of the San Andreas Flt, $L = 463$ km, and $x_c = 200.4$ km for Site 2

and $x_c = 57.3$ km for Site 3.

3.4 Uniform Hazard Motions

The results are presented in a form convenient for understanding the degree to which the

three contributors to the hazard affect the final result.   Spectra $SD(T,\zeta)$ as well as spectra

$SDC_L(T,\zeta,\tau)$ and $SDC_T(T,\zeta,\tau)$, which affect any site, not just those on a fault, are shown,

while the fault displacement hazard is shown separately. Damping ratio $\zeta = 5\%$ was assumed

and seismic exposure of 50 years.   The results are shown in Figs 6 through 17, in batches of four

figures for each site (Figs 7 through 9 for Site 1, Figs 10 through 13 for Site 2 and Figs 14

through 17 for Site 3). The first plot in each set (e.g. Fig. 6) shows $SD(T,\zeta;p,t)$ for horizontal

motions for five probabilities of being exceeded, $p = 0.01$, 0.1, 0.5, 0.9 and 0.99. It also shows

levels of horizontal fault displacement, assuming pure strike slip and bilateral rupture, with

probabilities of being exceeded $p = 0.01$, 0.1, 0.2, 0.3 if they exist. It is noted here that the

probability of exceeding certain level of fault displacement during the exposure does not

necessarily go to 1 even for very small levels.   As the results show, the probability that the fault

displacement exceeds given value is less than 0.4 for all three sites, and levels exist at most for

$p = 0.3$. The other three plots (e.g. Figs 7, 8 and 9) show $SD(T,\zeta;p,t)$ and $SDC_L(T,\zeta,\tau;p,t)$

and $SDC_T(T,\zeta,\tau;p,t)$ for a fixed value of p , set to 0.5, 0.1 and 0.01. If it exists, the level of

fault displacement with the same probability of being exceeded is also shown. In these plots,

$SD(T,\zeta;p,t)$ is shown by the heavier solid line, and appears as a backbone curve for the

$SDC(T,\zeta,\tau;p,t)$ spectra shown by weaker lines. The spectra for longitudinal motions,

$SDC_L(T,\zeta,\tau;p,t)$, are shown by the weaker solid lines, and those for transverse motions,

$SDC_T(T,\zeta,\tau;p,t)$, are shown by the weaker dashed lines.   Spectra for three values of τ are

sown, τ =0.1, 0.01 and 0.001.

It can be seen from Figs 6, 10 and 14, the $SD(T,\zeta;p,t)$, i.e. the relative displacement of a

structure due to dynamic response, increases rapidly with increasing period, reaching its

maximum at around $T = 3$ s for all three sites.   Therefore, the transient differential motions,

which do not depend on the structural period, are more significant for shorter period, i.e. stiffer

structures, and are practically not significant for structures with period T >1 s, which is clearly

seen in the figures showing $SDC_L(T,\zeta,\tau;p,t)$ and $SDC_T(T,\zeta,\tau;p,t)$.

The comparison of the hazard for permanent displacement, i.e. the fault displacement hazard,

with the hazard for the transient displacements shows the following.   As it can be seen from Figs

6, 10 and 14, for very small and equal probabilities of being exceeded, e.g. $p = 0.01$, the levels

of fault displacement are much higher than the values of $SD(T,\zeta;p,t)$ even at longer periods.

Therefore, for such small p, the hazard for relative displacement of columns is governed by the

fault displacement hazard.   However, for smaller values of p, the fault displacement hazard

becomes progressively less significant. As it can be seen from Fig. 8, e.g., for $p = 0.1$, at Site 1,

the hazard for $SDC_L(T,\zeta,\tau;p,t)$ and $SDC_T(T,\zeta,\tau;p,t)$ becomes more significant than the

fault displacement hazard for structures with periods longer than about 1s. For the same

probability, at Sites 2 and 3, however, the fault displacement still governs the hazard.   For

smaller p, however, e.g. $p = 0.5$, the differential motion (at shorter periods) and the spectral

displacement (at longer periods) govern the hazard at all three sites.
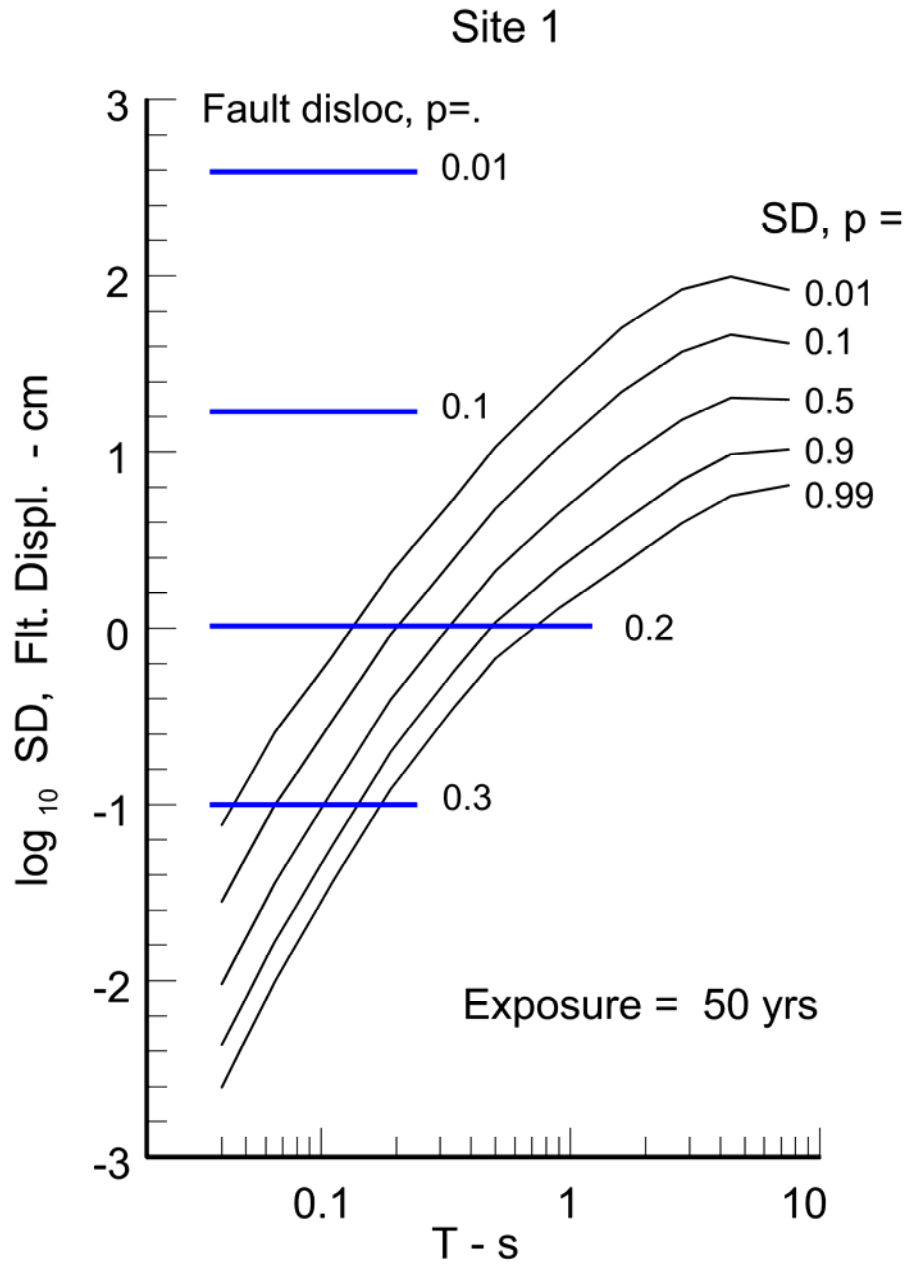
Fig. 6 Site 1: Uniform Hazard Spectral Displacement $SD(T)$ for $\zeta = 5\%$ and for probabilities of being exceeded $p = 0.01$, 0.1, 0.5, 0.9 and 0.99 in 50 years. The Fault Displacement levels for probabilities of being exceeded $p = 0.01$, 0.1, 0.2 and 0.3 are also shown.
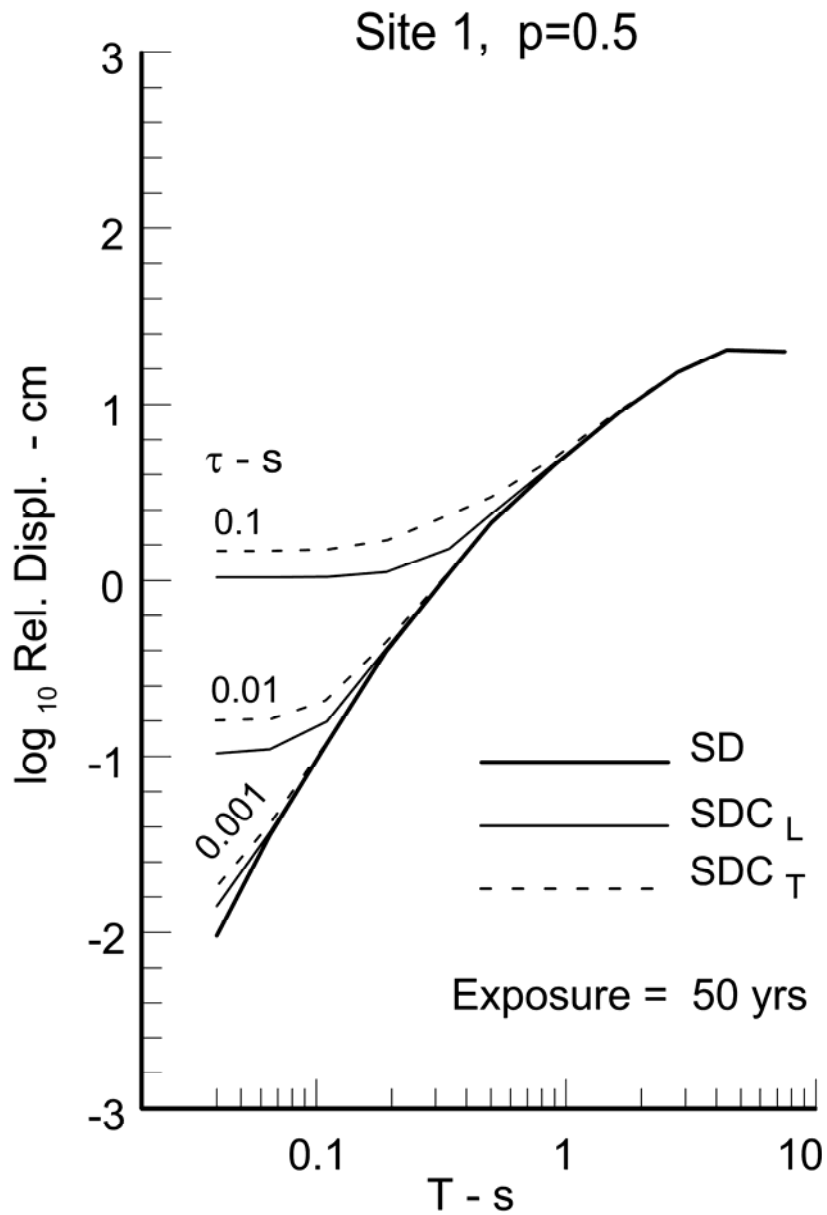
Fig. 7   Site 1: Spectral Displacement $SD(T)$, and Spectral Displacement for Columns for longitudinal and transverse motions, $SDC_L(T,\zeta,\tau)$ and $SDC_T(T,\zeta,\tau)$ for $\zeta = 5\%$ and for probability of being exceeded $p = 0.5$ in 50 years.
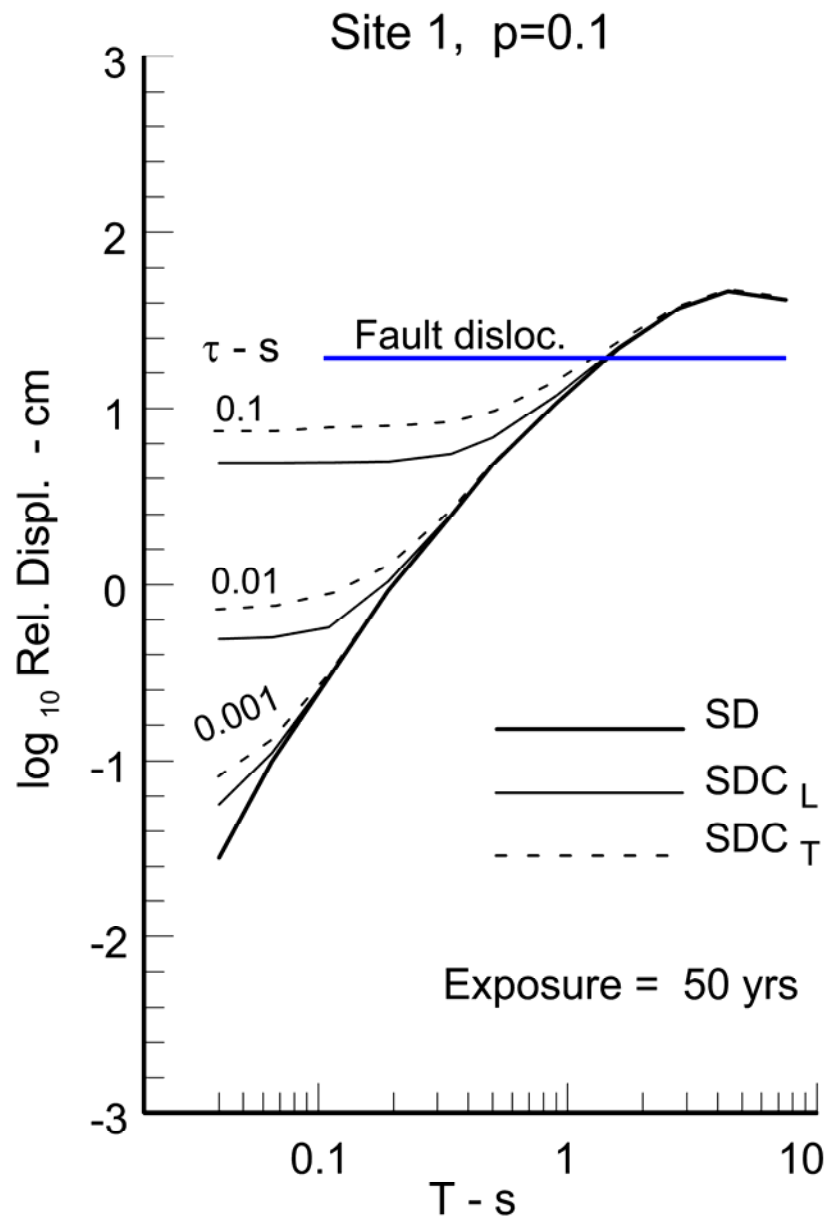
22

Fig. 8 Same as Fig. 7 but for probability of being exceeded $p = 0.1$ in 50 years. The Fault Displacement level for the same probability is also shown.
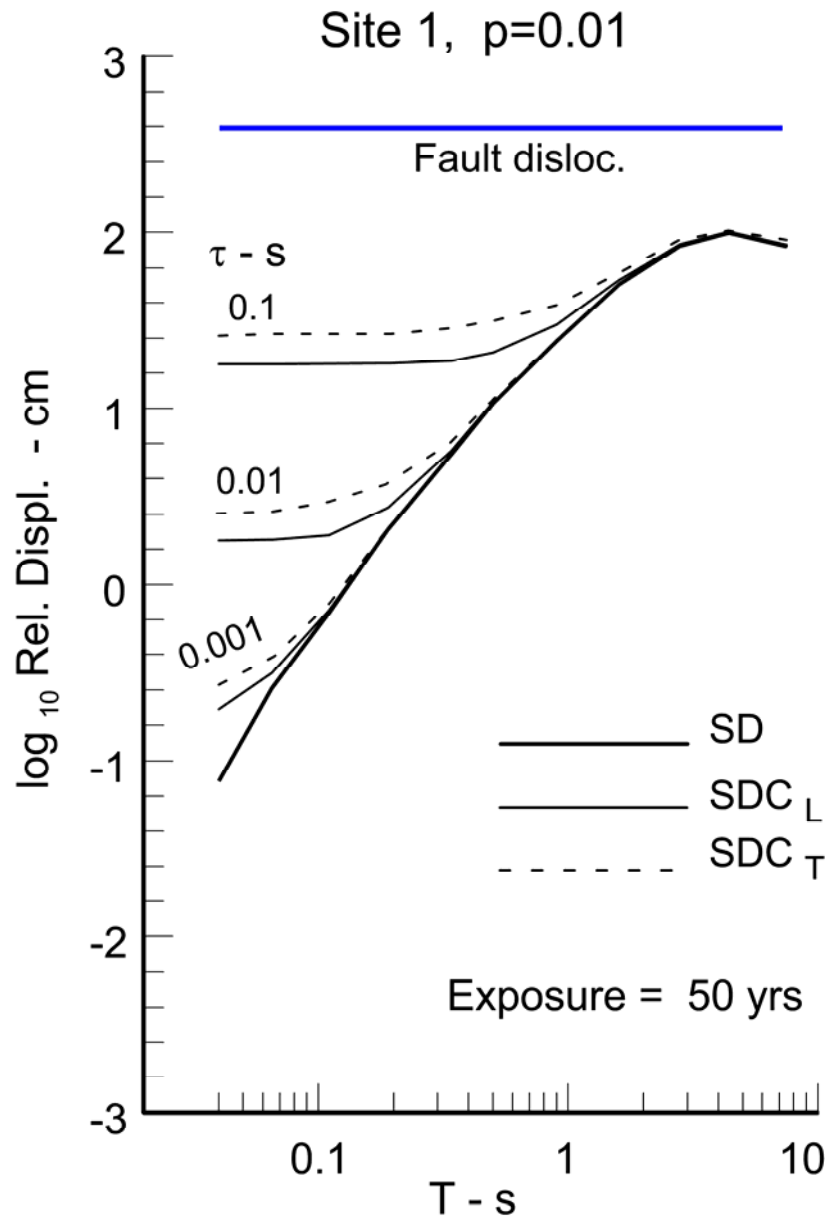
Fig. 9 Same as Fig. 7 but for probability of being exceeded $p = 0.01$ in 50 years. The Fault Displacement level for the same probability is also shown.
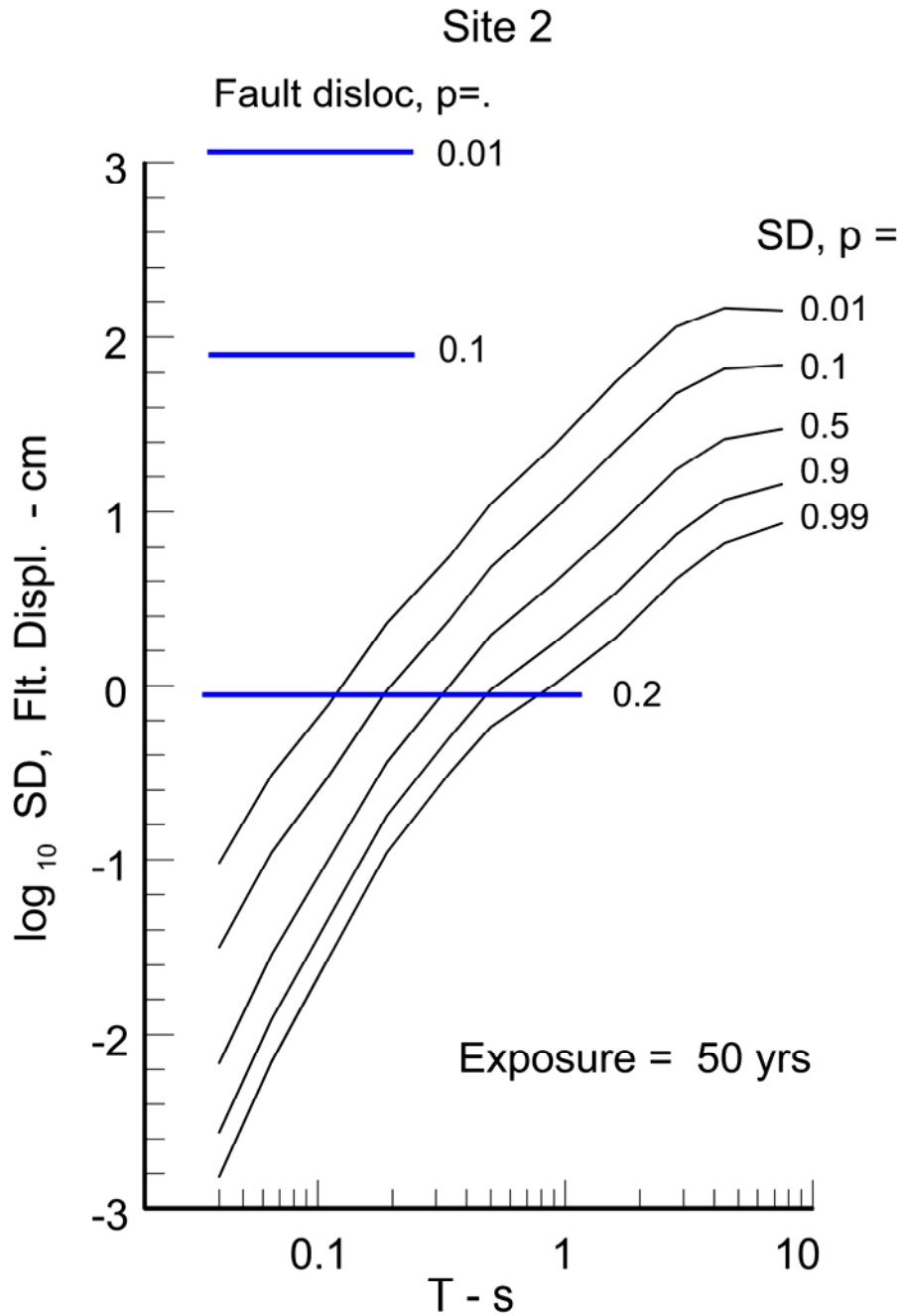
24

Fig. 10 Site 2: Uniform Hazard Spectral Displacement $SD(T)$ for $\zeta = 5\%$ and for probabilities of being exceeded $p = 0.01$, 0.1, 0.5, 0.9 and 0.99 in 50 years. The Fault Displacement levels for probabilities of being exceeded $p = 0.01$, 0.1, 0.2 and 0.3 are also shown.
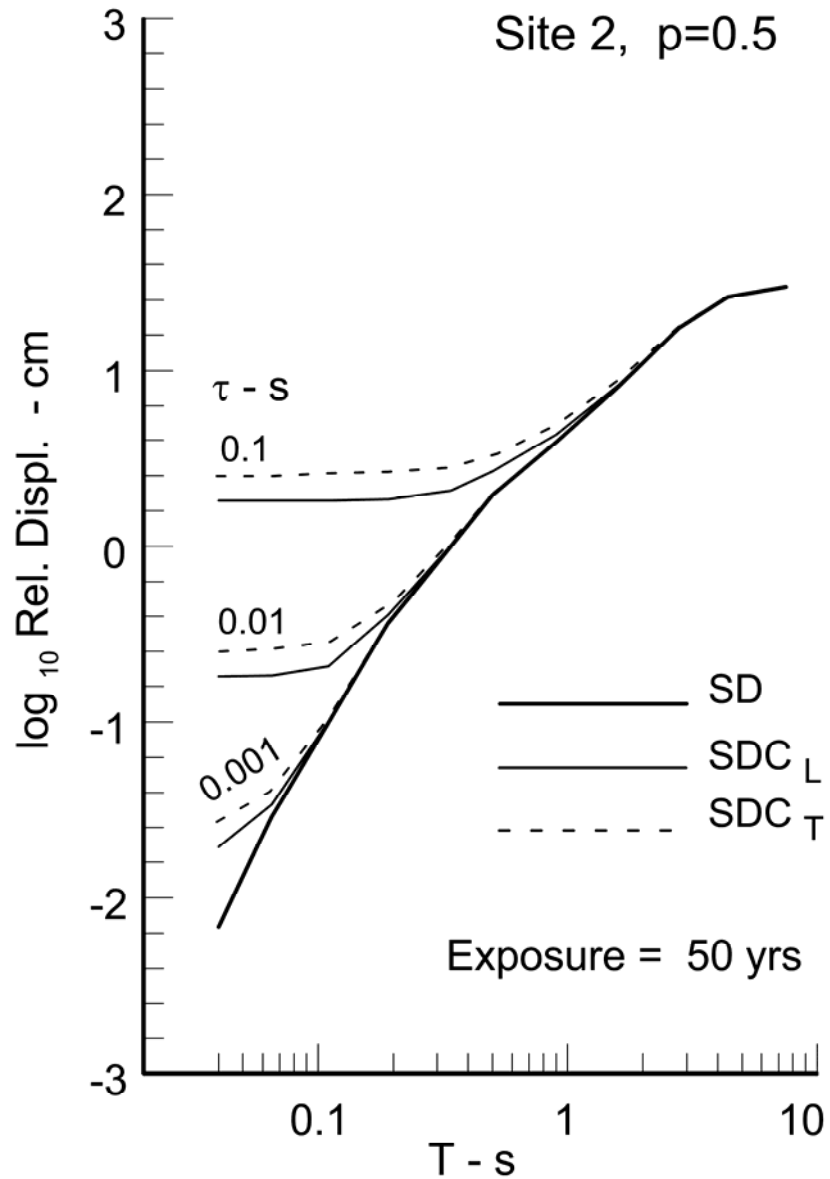
Fig. 11   Site 2: Spectral Displacement $SD(T)$, and Spectral Displacement for Columns for longitudinal and transverse motions, $SDC_L(T,\zeta,\tau)$ and $SDC_T(T,\zeta,\tau)$ for $\zeta = 5\%$ and for probability of being exceeded $p = 0.5$ in 50 years.
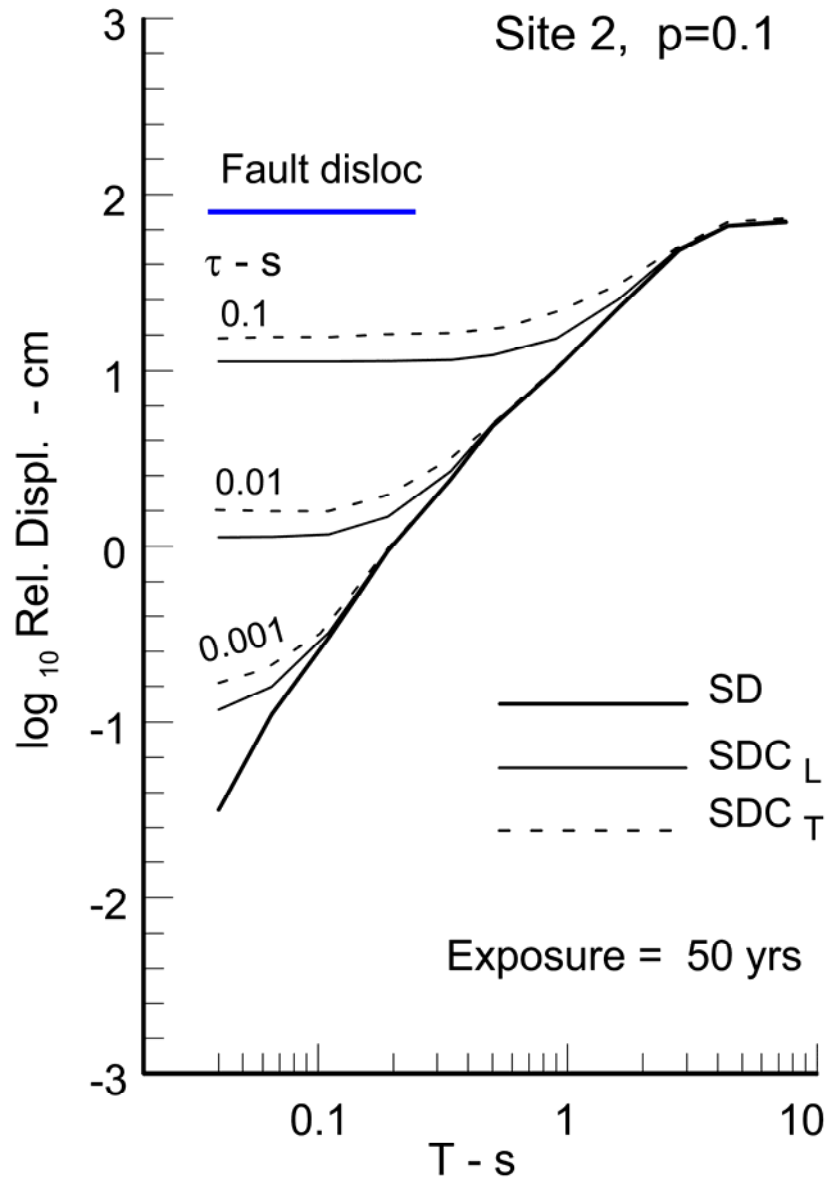
26

Fig. 12   Same as Fig. 11 but for probability of being exceeded $p = 0.1$ in 50 years. The Fault Displacement level for the same probability is also shown.
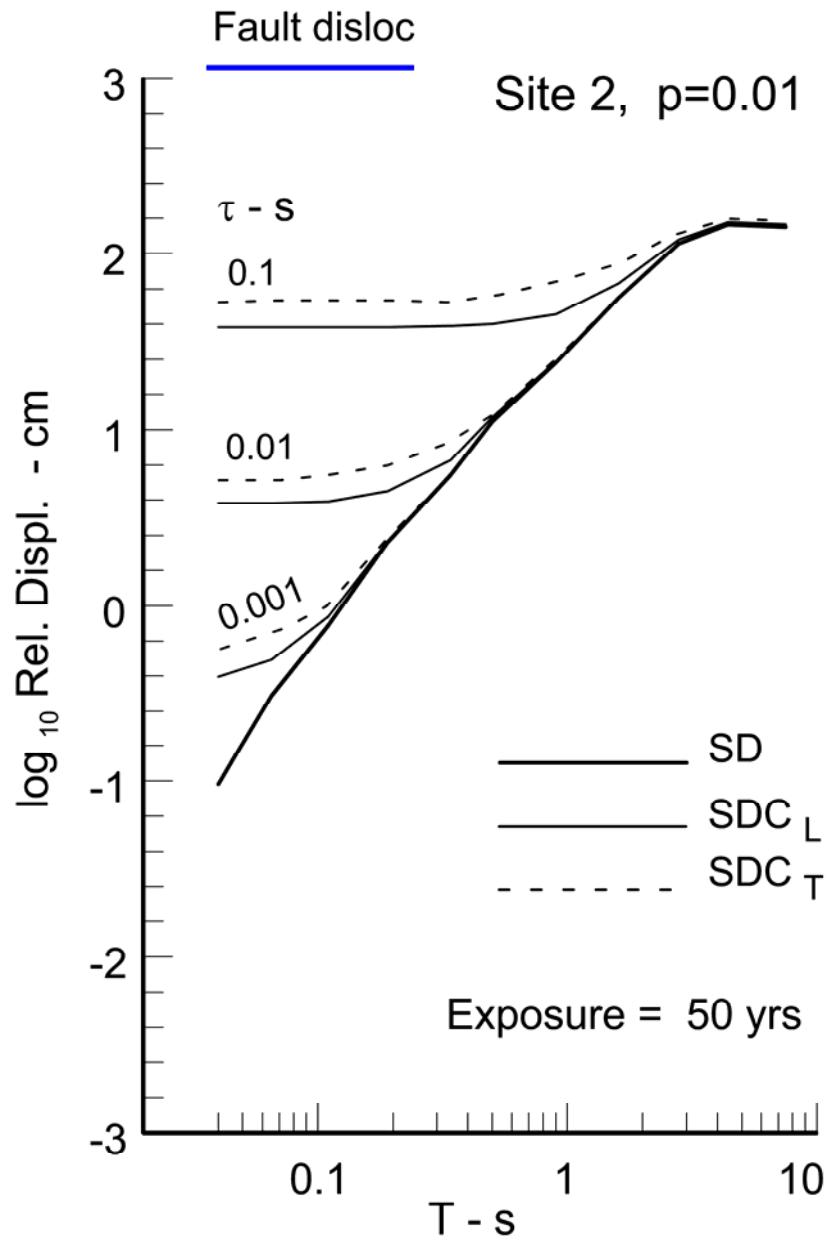
Fig. 13 Same as Fig. 11 but for probability of being exceeded $p = 0.01$ in 50 years. The Fault Displacement level for the same probability is also shown.

Fig. 14 Site 3: Uniform Hazard Spectral Displacement $SD(T)$ for $\zeta = 5\%$ and for probabilities of being exceeded $p = 0.01$, 0.1, 0.5, 0.9 and 0.99 in 50 years. The Fault Displacement levels for probabilities of being exceeded $p = 0.01$, 0.1, 0.2 and 0.3 are also shown.

Fig. 15 Site 3: Spectral Displacement $SD(T)$, and Spectral Displacement for Columns for longitudinal and transverse motions, $SDC_L(T,\zeta,\tau)$ and $SDC_T(T,\zeta,\tau)$ for $\zeta = 5\%$ and for probability of being exceeded $p = 0.5$ in 50 years.

Fig. 16 Same as Fig. 15 but for probability of being exceeded $p = 0.1$ in 50 years. The Fault Displacement level for the same probability is also shown.

Fig. 17 Same as Fig. 15 but for probability of being exceeded $p = 0.01$ in 50 years. The Fault Displacement level for the same probability is also shown.
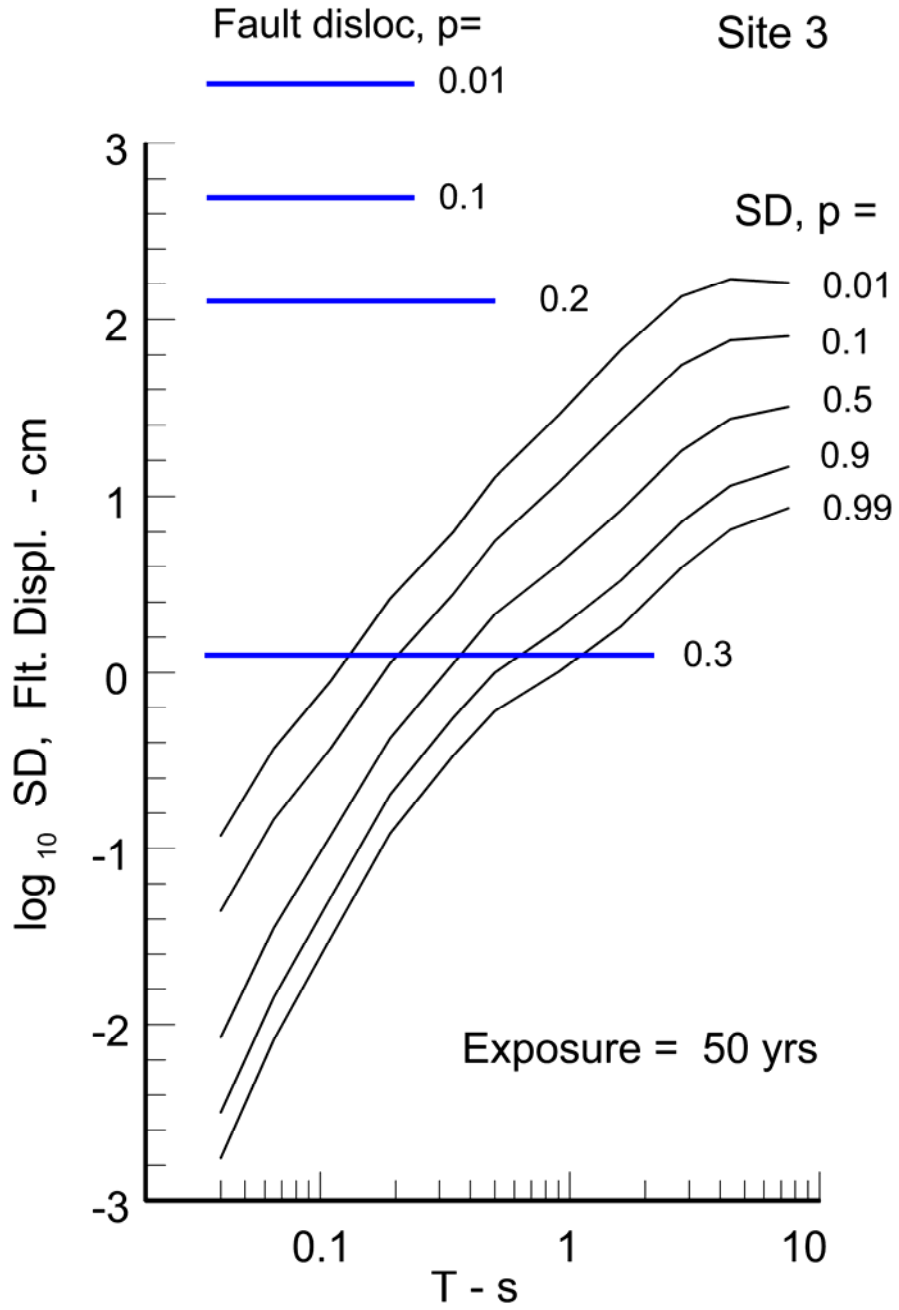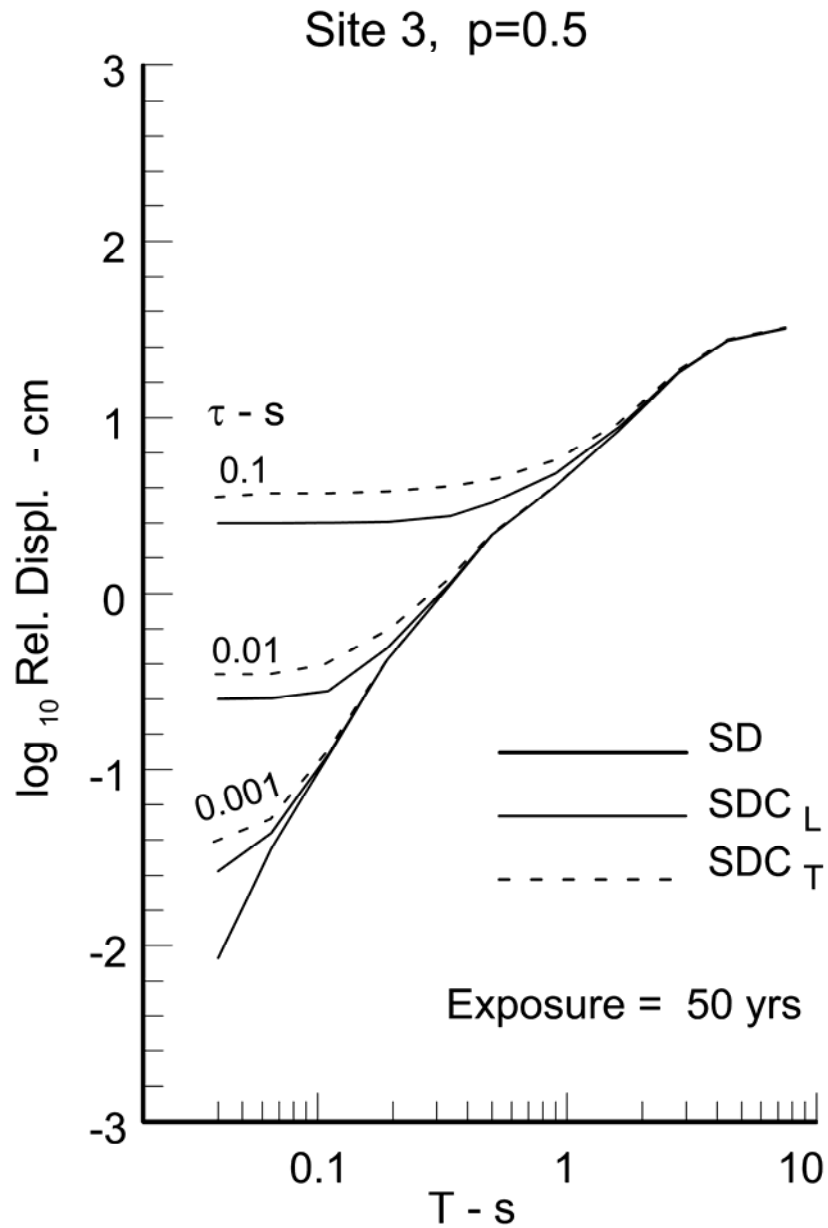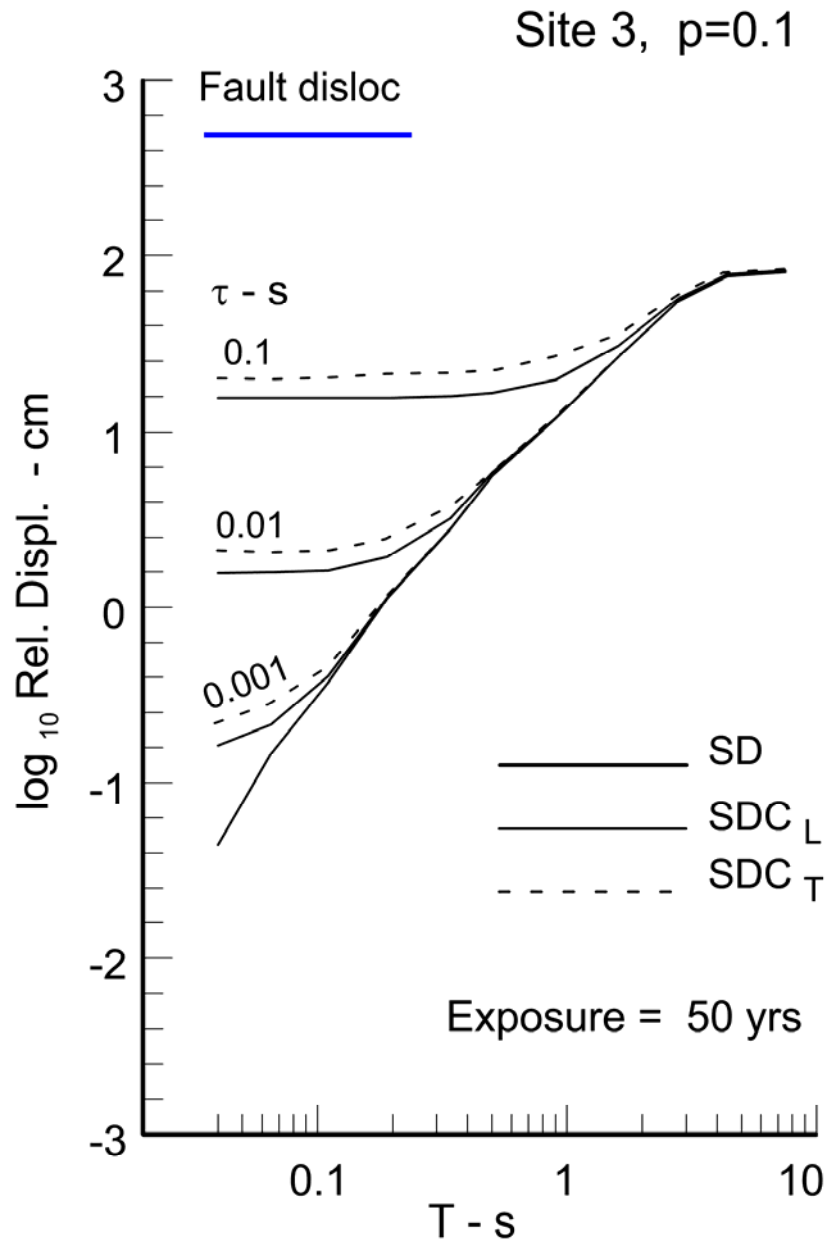
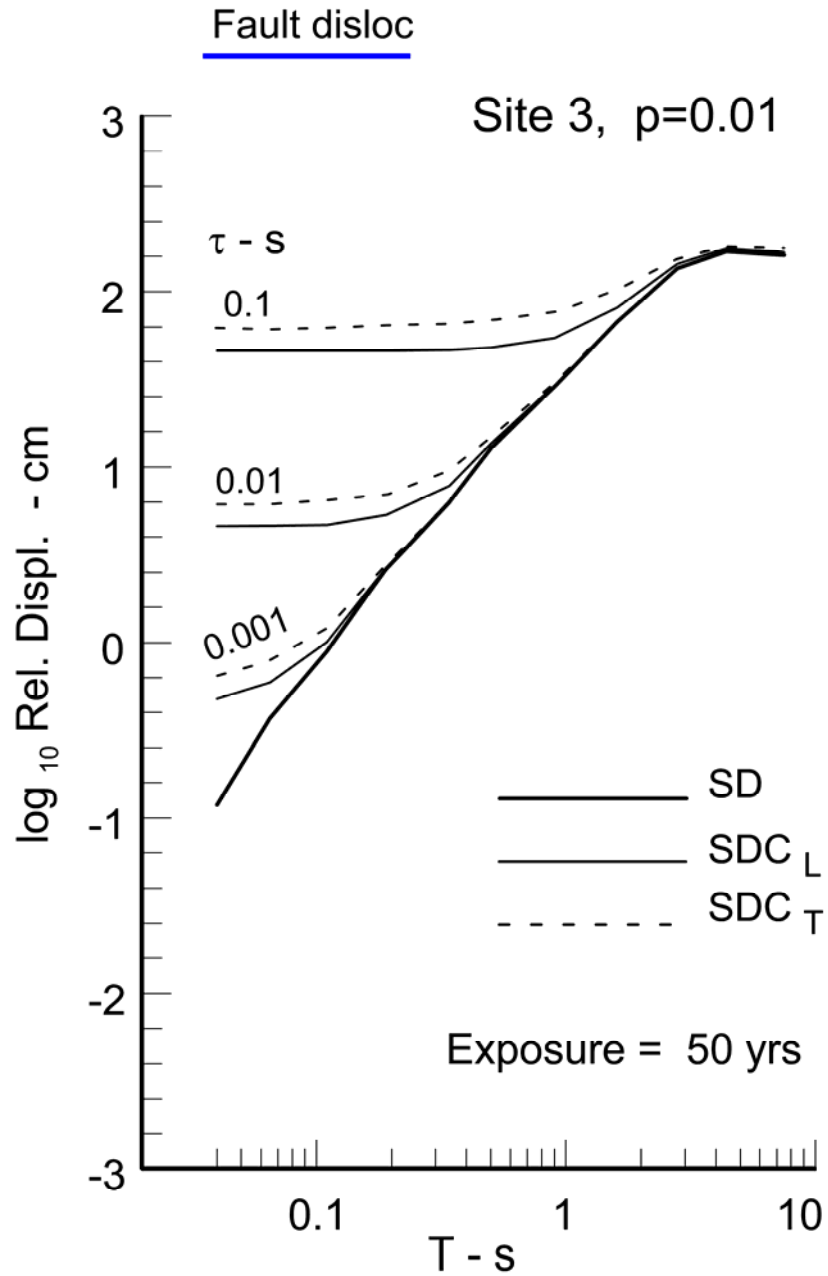# 4.   DISCUSSION AND CONCLUSIONS

A methodology was presented and illustrated for prediction of the peak relative displacement of columns of bridge structures, caused by earthquakes, which considers the following three effects: (i) relative displacement due to dynamic forces, which depends on the period of vibration of the structure, (ii) transient differential motions (on level ground) caused by ground strains, and (ii) static differential motions caused by fault offset. The methodology is probabilistic and is formulated within the framework of Probabilistic Seismic Hazard Analysis (PSHA). The methodology was demonstrated for three sites in Southern California, for a hypothetical seismicity model, and using existing scaling models for response spectra, peak ground velocity and fault displacement. All sites lie on a fault. Uniform hazard relative displacement spectra $SDC(T,\zeta,\tau;p,t)$ were computed, which combine the effect of the transient motions, and were compared with the permanent relative displacements caused by fault offset, for the same confidence levels.

The results show that, for the particular seismicity model used, the levels of the predicted peak relative displacement amplitudes depend on the probability that these levels will be exceeded during the seismic exposure period (life of service time of the structure), on the location of the site relative to the seismic sources in the region, and, for the fault displacement, also on how centrally the site is located on the fault.   The transient peak relative displacements, $SDC(T,\zeta,\tau;p,t)$, also strongly depend on the structural period, T, and on the length of the structure and wave speeds in the soil near the surface (through the time delay parameter, τ).

Based on this study, the following conclusions are drawn about the peak transient relative displacements. Generally, for longer period (more flexible) structures (T greater than about 1 s),

the dynamic response dominates $SDC(T,\zeta,\tau;p,t)$, while, for shorter period (stiffer) structures (T less than about 1 s), the differential motions are significant and must be considered for design.

For a structure that crosses a fault, the relative significance of the fault displacement hazard depends strongly on the confidence level of the prediction. For very small probability of being exceeded ($p = 0.01$ in this study), the levels of static displacement caused by fault offset are much higher than the levels of $SDC(T,\zeta,\tau;p,t)$ and the fault displacement controls the hazard. However, as p increases, the level of fault displacement that will be exceeded rapidly decreases and eventually becomes smaller than $SDC(T,\zeta,\tau;p,t)$ for some value of p. The value of p at which this happens depends on the site location and seismicity model. For the examples considered in this study, for Sites 2 and 3, even for $p = 0.1$ the static displacements are the largest and the fault displacement governs the hazard. For Site 1, the fault displacement governs the hazard only for shorter period structures. For $p = 0.5$, however, the transient displacements govern the hazard.

The level of p to be used in selecting design motion for a particular structure will depend on the importance of the structure. Based on this study, the fault displacement hazard is more likely to affect the design ground motions for important bridges. For less important bridges, the design ground motion are more likely to be determined by the $SDC(T,\zeta,\tau)$. For a particular structure, site specific PSHA calculations should be performed, using the most current information on the earthquake sources and scaling models. The examples in this study are hypothetical, and meant to be used only for the purpose of demonstrating the methodology, and understanding the interplay between the different processes, and should not be used for the design of a particular structure. It is also noted that other factors contributing to differential motion, such as, e.g.,

differences in topography and soil conditions along the supports of the structure, and lateral spreading caused by liquefaction, which may be important for some structures, were not considered in this study.

5. REFERENCES

1. Anderson J.G., Trifunac M.D. (1978). Uniform risk functionals for characterization of strong earthquake ground motion, *Bull. Seism. Soc. Amer.*, **68**, 205-218.

2. Lee V.W. (2002). Empirical scaling of strong earthquake ground motion: part I: attenuation and scaling of response spectra, *ISET J. Earthquake Technology*, **39**(4), 219-254.

3. Lee V.W., Trifunac M.D. (1985) Pseudo Relative Velocity Spectra of Strong Earthquake Ground Motion in California, *Dept. of Civil Eng. Report No. CE 95-04*, Univ. of Southern California, Los Angeles, California.

4. Lee V.W., Trifunac M.D. (1995). Pseudo Relative Velocity Spectra of Strong Earthquake Ground Motion in California, *Dept. of Civil Engrg Report No CE 95-04*, Univ. of Southern California, Los Angeles, California.

5. Lee V.W., Trifunac M.D. (1987). Microzonation of a metropolitan area, *Dept. of Civil Engrg, Report CE 87-02*, Univ. of Southern California, Los Angeles, California.

6. Lee V.W., Trifunac M.D. (2010). Should average shear-wave velocity in the top 30 m of soil be used to describe seismic amplification? *Soil Dynamics & Earthquake Engrg*, 30, 1250–1258.

7. Lee V.W., Trifunac M.D., Todorovska M.I., Novikova E.I. (1995). Empirical equations describing attenuation of horizontal peaks of strong ground motion in terms of magnitude, distance, path effects and site conditions, *Dept. of Civil Engrg. Report No. 95-02*, Univ. of Southern California, pp. 409.

8. Todorovska M.I., Trifunac M.D. (1996). Hazard mapping of normalized peak strain in soil during earthquakes: microzonation of a metropolitan area, *Soil Dynamics & Earthquake Engrg*, **15**(5), 321-329.

9. Todorovska M.I., Trifunac M.D. (1999). Liquefaction opportunity mapping via seismic wave energy, *J. Geotechnical and Geoevironmental Engrg*, ASCE, **125**(12), 1032-1042.

10. Todorovska M.I., Trifunac M.D. (2006). Probabilistic fault displacement hazard for the transportation system, *Proc. 8th National Conf. on Earthquake Engineering*, 100th Anniversary Earthquake Conference, San Francisco, California, April 18-22, 2006, pp. 10.

11. Todorovska M.I., Trifunac M.D., Lee V.W. (2007). Shaking hazard compatible methodology for probabilistic assessment of permanent ground displacement across earthquake faults, *Soil Dynamics & Earthquake Engrg*, **27**(6), 586–597.

12. Trifunac M.D. (1976). Preliminary analysis of the peaks of strong earthquake ground motion-dependence of peaks on earthquake magnitude, epicentral distance and the recording site conditions, *Bull. Seism. Soc. Amer.*, **66**(1), 189-219, pp.30, 1976.

13. Trifunac M.D. (1978). Response spectra for earthquake ground motion, *ASCE EM5*, **104**, 1081-1097.

14. Trifunac M.D. (1990). A microzonation method based on uniform risk spectra, *Int. J. Soil Dynamics & Earthquake Engrg*, **9**(1), 34-43, 1990.

15. Trifunac M.D., Lee V.W. (1989). Empirical models for scaling pseudo relative velocity spectra of strong earthquake accelerations in terms of magnitude, distance, site intensity and recording site conditions, *Int. J. Soil Dynamics & Earthquake Engrg*, **8**(3), 126-144.

16. Trifunac M.D., Todorovska M.I. (1997). Response spectra for differential motion of columns, *Earthquake Engrg & Struct. Dynamics*, **26** (2), 251-268.

17. Trifunac M.D., Gičev V. (2006). Response spectra for differential motion of columns, paper II: out-of-plane response, *Soil Dynamics & Earthquake Engrg*, **26**(12), 1149-1160.

18. Wells D.L., Coppersmith K.J. (1994). New empirical relationships among magnitude, rupture length, rupture width, rupture area, and surface displacement, *Bull. Seism. Soc. Amer.*, **84**(4), 974-1002.

19. Working Group on California Earthquake Probabilities (1995). Seismic hazards in southern California: Probable earthquakes, 1994 to 2024. *Bull. Seism. Soc. Amer.*, **85**(2), 379–439.